pH-Responsive porphyrin-silica nanoparticles conjugate *via* ionic self-assembly

Maher Fathalla[*a,b,c] and Lutfan Sinatra[a]

[a] Division of Physical Sciences and Engineering, Solar and Photovoltaics Engineering Center, King Abdullah University of Science and Technology (KAUST), Thuwal 23955-6900, Saudi Arabia.

[b] Department of Chemistry, Faculty of Science, Zagazig University, Zagazig 44519, Egypt

[c] Department of Chemistry, Faculty of Science, Islamic University of Madinah, Madinah 170, Saudi Arabia

Corresponding author email address: mfathalla@zu.edu.eg

Abstract

Ionic self-assembly (ISA) is a powerful tool that has been exploited to create various functional nanomaterials through the electrostatic interactions of different building blocks. Herein, we disclose for the first time the synthesis and characterization of benzoic acid functionalized silica nanoparticles (MSN-Bn) and its subsequent ISA with meso-tetrakis(N-methylpyridinium-4-yl)porphyrin (TMPyP) to form a pH responsive hybrid material. The resulting pH responsive conjugate is an attractive candidate as a drug delivery vehicle in which the MSN-Bn act as a drug carrier and the TMPyP act as a capping agent for the silica nanopores. The application of these pH-responsive interactions between the negatively charged carboxylate groups on the surface of mesoporous silica nanoparticles and the positively charged porphyrin as a drug delivery system was investigated by studying the loading and release of Hoechst 33342 dye (a water-soluble biological stain with similar size to those of therapeutic drugs) in response to a pH change. The reported approach enables the delivery of a chemotherapeutic drug in addition to the TMPyP, which is also well-known as a photodynamic therapy (PDT) agent, thus paving the way for synergistic chemo-photodynamic cancer therapy. The study shows that the resulting conjugate demonstrate the drug delivery mechanism which is responsive to changing the pH values from 7.5 to 4.5, and can deliver about 2wt% of the chemotherapeutic drug tested.

Keywords Porphyrin. Silica Nanoparticles. Drug Delivery. Photodynamic Therapy. Ionic self-assembly

1 Introduction

The development of an efficient treatment for cancer is the ultimate goal of many biomedical researchers worldwide. Photodynamic therapy (PDT) is an attractive approach for the treatment of a number of diseases including cancer[1–5]. PDT is based on the generation of singlet oxygen ($^1O_2$) species from a photosensitizer upon light irradiation. The produced $^1O_2$ species cause cell death of specific cellular targets without damaging the surrounding healthy tissues. Since the photosensitizer plays a vital role in PDT outcomes, its selection is critical for efficient PDT treatment. Amongst the available photosensitizers, meso-tetrakis(N-methylpyridinium-4-yl) porphyrin (TMPyP) received considerable attention due to (i) its high water solubility, (ii) its high capacity to penetrate plasma membrane and generate $^1O_2$, and (iii) its tendency to bind to G-quadruplex formed by guanine rich DNA and RNA sequences. Furthermore, various studies have shown the anti-cancer capability of TMPyP through its ability to inhibit telomerase enzyme by stabilizing G-quadruplex structures through external stacking onto guanine nucleobases [6–16]

Chemotherapy is another approach to treat cancer. However, a serious drawback of this method is the side effects of the used chemo-therapeutic agent on the healthy cells as a result of non-targeting delivery [17]. In order to circumvent this problem, nano-carriers have recently been developed in order to encapsulate and deliver the anti-cancer drug to the target cells with high selectivity. Among the developed nano-carriers, mesoporous silica nanoparticles (MSN) [17–28] have shown great potential for applications in drug delivery vehicles due to its biocompatibility, high surface area, and tendency to undergo cellular uptake into acidic lysosomes by endocytosis when having a diameter of 100-200 nm. Consequently, several drug delivery systems based on MSNs have been developed during the last decade [29–42]. In these systems, controlled release of drug can be achieved in response to various stimuli such as light, redox potential, temperature, pH and enzymes. Since the tumour cells have a more acidic environment compared to the normal cells, the pH responsive MSN nano-carriers provide an efficient strategy to deliver anti-cancer drugs.

Various pH responsive MSN have been developed using different capping agents, such as polymer, biomolecules and also inorganic nanoparticles [37,38,43–50] The challenge here is to find the responsive capping agent that can effectively release the drug selectively on the cancer cells. Porphyrin have been studied intensively for PDT agent. The selective delivery of porphyrins to the infected cells is a major obstacle in applying them as photosensitizers. Consequently, the design of pH-responsive materials that encompass both MSN and porphyrin is a potential approach to circumvent this challenge. Utilizing porphyrin as a capping agent on MSN and also PDT agent in the same time will result in more efficient drug delivery system.

Recently, synergistic therapy has emerged as an efficient strategy to treat cancer [51–56]. In this approach, nanoparticles with two or more therapeutic agents are delivered to the cancer cells causing more efficient cell apoptosis. Using the similar approach, combining different cancer treatment such as PDT and chemotherapeutic will increase the efficiency of the method to kill cancer cell. In this work, we decided to combine the advantages of TMPyP (as PDT agent) with MSNs (as a drug carrier). It is envisioned that the TMPyP-MSN conjugate will have both the light-mediated cell killing properties of the porphyrin photosensitizer and the tendency to deliver additional chemo-therapeutic drugs to the target cells which will lead to an efficient chemo-photodynamic therapy for cancer. In order to combine all these system, we designed and synthesized benzoic acid functionalized silica nanoparticles (MSN-Bn) and combined it with TMPyP as a capping agent via ionic self-assembly to form porphyrin-MSN conjugate capable of releasing a cargo in response to a pH change. The study shows that the resulting conjugate demonstrate the drug delivery mechanism which is responsive to changing the pH values from 7.5 to 4.5, and can deliver about 2wt% of the chemotherapeutic drug tested.

2 Experimental

Synthesis of Mesoporous Silica Nanoparticles (MSNs) [57].

Cetyltrimethylammonium bromide [CTAB] (0.5 g) and 3.4 g of Pluronic F127 were dissolved in 96 mL of distilled water, 34 g (43 mL) EtOH, and 10.05 g (11.16 mL) of 29 wt % ammonium hydroxide solution at room temperature (RT). After complete dissolution, 1.8 g (1.935 mL) tetraethyl orthosilicate (TEOS) was added into the mixture at once. After 1 min of mechanical stirring at 1000 rpm, the mixture was kept at a static condition for 24h at RT for further silica

condensation. The white solid product is recovered by ultrahigh speed centrifuge, washed several times with methanol and dried overnight under vacuum.

Amino functionalization of mesoporous silica nanoparticles (MSNs-NH_2).

0.3g as-made MSNs were suspended in anhydrous toluene (30 ml), 0.75 ml (3-aminopropyl)triethoxysilane (APTES) was added to the mixture. The solution was refluxed for 24 h. It was cooled down to room temperature, and the product were centrifuged, washed thoroughly with MeOH, and dried at room temperature overnight.

Removal of CTAB.

Amino functionalized MSNs (0.3 g) were suspended in MeOH (75 mL), to which a concentrated aqueous solution of HCl (12M, 4 mL) had been added, and the mixture was heated under reflux for 24 h. the solvent-extracted nanoparticles were collected by vacuum filtration and washed thoroughly with MeOH.

Synthesis of MSNs-benzoate.

a) Synthesis of methyl (4-iodomethyl)benzoate [58].

A solution of 5 gm of methyl (4-bromomethyl) benzoate in 10 mL of acetone was added a solution of 6.6 gm of sodium iodide in 15 mL of acetone, and the mixture was refluxed for 40 minutes. The sodium bromide was removed by filtration, the acetone was distilled and the residue was taken up in ether. The ether solution was washed with water and dried over anhydrous magnesium sulfate. Then ether was removed under reduced pressure to give methyl (4-iodomethyl) benzoate.

b) Synthesis of MSNs-benzoate.

100 mg of MSNs-NH_2 and 100 mg of methyl (4-iodomethyl) benzoate were dissolved in 5mL toluene and 0.5mL diisopropyl ethylamine was added to the mixture. The reaction mixture was then heated under reflux for 24h. Subsequently, it was cooled down to room temperature, and the product were centrifuged, washed thoroughly with MeOH, and dried at room temperature overnight.

Synthesis of MSNs-benzoic acid (MSNs-Bn)

To 60 mg of benzoate functionalized MSNs in 60 mL distilled water was added 3 mL conc HCl and the mixture was heated under reflux for 24 h. The solvent-extracted nanoparticles were collected by vacuum filtration and washed thoroughly with MeOH until the supernatant pH is 7.

Hoechst 33342 loading to MSNs-Bn.

10 mg of benzoic acid functionalized MSNs (MSNs-Bn) were added to 1 mL (1mM) of Hoechst 33342 (in ethanol) and the mixture was stirred overnight at room temperature. The MSNs-Bn loaded with Hoechst 33342 was then separated by centrifugation (15000 rpm/3min) washed with either water or ethanol and dried under vacuum overnight.

Capping MSNs-Bn nanopores with TMPyP.

3 mg of meso-tetrakis(N-methylpyridinium-4-yl)porphyrin (TMPyP) was added to a suspension of a Hoechst-loaded MSN-Bn (10 mg) in a buffered solution (Tris buffered, pH 7.5) and the mixture was stirred overnight. The assembled mechanized nanoparticle was collected by centrifugation (15000 rpm/3min) washed with distilled water until the washing no longer exhibited fluorescence, and dried under vacuum overnight.

pH-Controlled storage-release experiments.

To Hoechst-loaded, TMPyP capped MSNs-Bn nanoparticles (2 mg) were placed in aqueous solution at different pH (either 7.5 or 4.5) and stirred at constant rate. The fluorescence emission of the supernatant fluid was measured at predetermined time intervals, then the liquid was poured back to maintain the total volume of the suspension.

3 Results and discussion

The benzoic acid functionalized silica nanoparticles (MSNs-Bn) **1** were synthesized according to scheme **1**. First, MSNs were synthesized with a base-catalyzed sol-gel method using tetraethyl orthosilicate (TEOS) as silica source and cetyltrimethylammonium bromide (CTAB) as templates [42]. The amino functionalization of MSNs was achieved by reaction with (3-aminopropyl)triethoxysilane (APTES) to afford **3**. CTAB template inside the mesopores was then

removed by refluxing with acidic solution in methanol. The modification of MSNs with APTES before removing the template prevents the functionalization of the internal surface of the pores leaving them accessible to the drug molecules. The benzoate functionalized MSNs **2** were achieved through refluxing **3** with methyl (4-iodomethyl)benzoate in toluene for 24 h to give **2** as a yellowish solid. Eventually, acid hydrolysis of the benzoate ester of **3** afforded benzoic acid functionalized silica nanoparticles (MSNs-Bn) **1** as off-white solid.

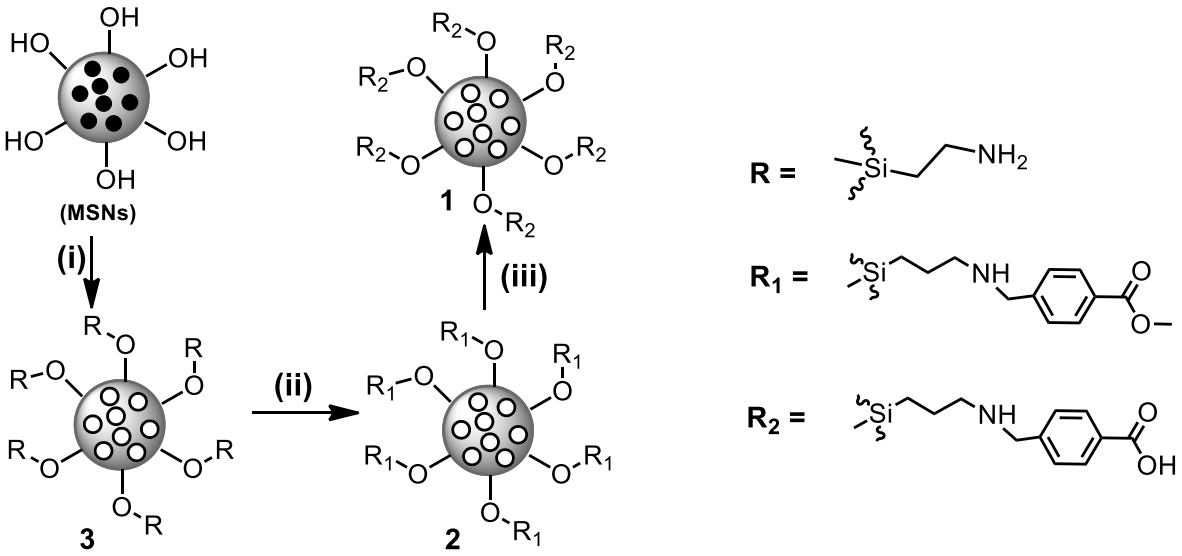

Scheme 1. Synthesis of MSNs-Bn **1**, (i) APTES/toluene, reflux for 24h then HCl/MeOH, reflux for 24h, (ii) methyl (4-iodomethyl) benzoate, DIPEA, reflux for 24h, (iii) HCl/H_2O, reflux for 24h.

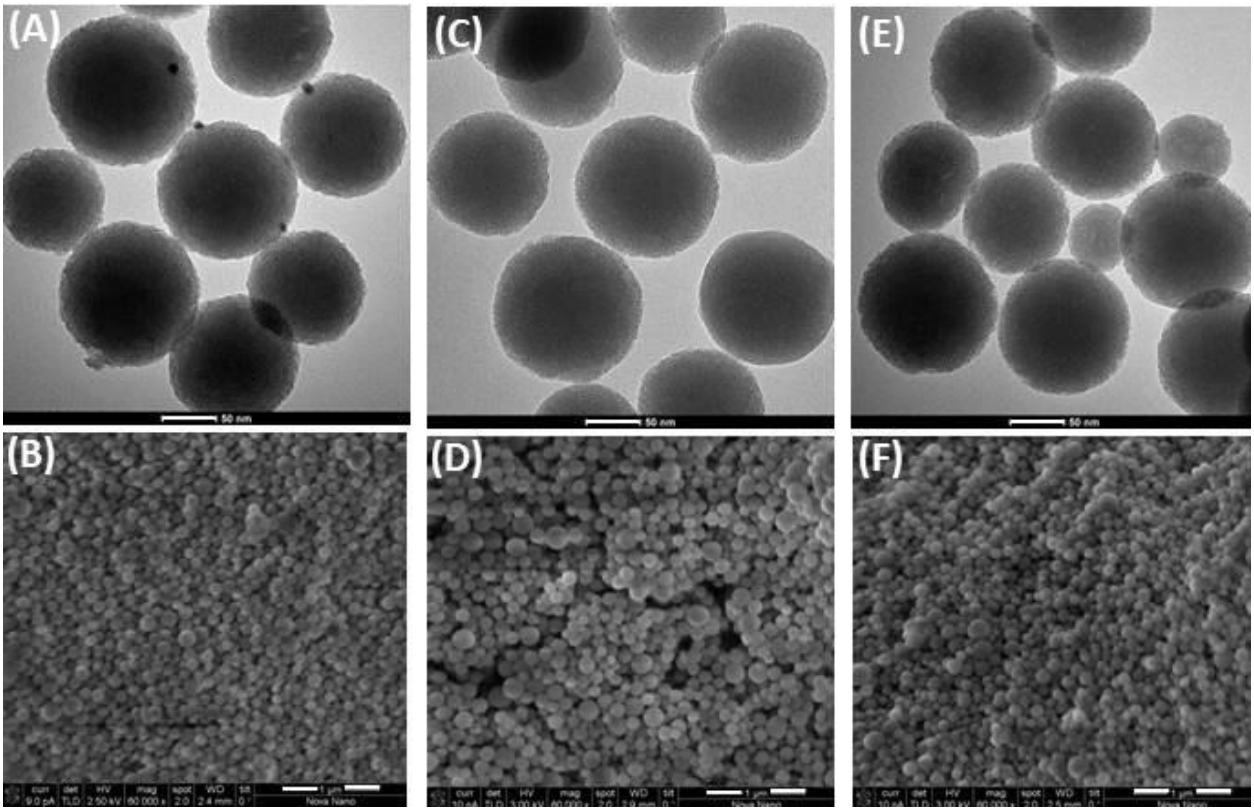

Fig. 1 TEM and SEM images of MSNs (A,B), MSNs-benzoate **2** (C,D) and MSNs-Benzoic acid **1** (E,F). (Scale bar for TEM is 50 nm and 1μm for SEM).

Scanning Electron Microsccopy (SEM) as well as Transmission Electron Microscopy (TEM) were used to investigate the morphology of the synthesized silica nanoparticle derivatives during the course of the reactions. As shown in Figure 1 and Figure S1 (Supporting Information), the prepared MSNs were uniform spherical with a mean diameter of approximately 100 nm. In addition, as shown in the TEM images, the MSNs retained its morphology during the course of the above-mentioned functionalization and hydrolysis procedures.

FT-IR spectra of the synthesized MSNs without removing the CTAB template (Figure 2) shows the characteristic C-H stretching vibrations of CTAB molecules at 2926 and 2855 cm^{-1} and C-H deformation at vibration around 1474 cm^{-1}. After removing CTAB template, the disappearance of the above-mentioned vibrational peaks was observed (Supporting Information, Figure S2). The successful APTES functionalization of MSNs to form **3** was confirmed through the appearance of N-H stretching vibrations at 3300 cm^{-1} (broad peak) as well as N-H bending vibration at 1625 cm^{-1}. The benzoate functionalization of **3** was confirmed by the presence of the C=O stretching

vibration at 1720 cm^{-1}, as well as, stretching vibration 1610 cm^{-1} associated with the C=C stretch in phenyl group (Supporting Information, Figure S2). Furthermore, the hydrolysis of benzoate ester was confirmed by IR through the emergence of a broad band at 3225 cm^{-1} corresponding to the O-H stretching vibration.

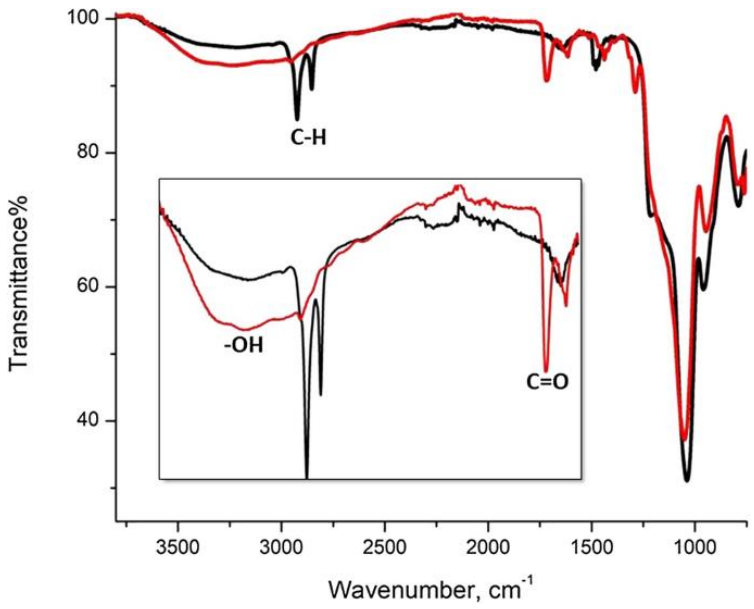

Fig. 2 FT-IR spectra of MSNs (black) and MSN-Bn **1** (red), Inset spectra show emergence of C=O and OH stretching frequencies after the functionalization of MSNs with benzoic acid as well as the disappearance of C-H stretching vibrational peaks of CTAB molecules.

The grafted amount of benzoate on MSNs was investigated by Thermogravimetric Analysis (TGA) study. As shown in Figure 3 (A), heating a sample of **2** to 750 ^{o}C showed an initial weight loss of *ca*. 9% that can be attributed to the loss of trapped solvents, followed by a 24% loss for the organic contents of the benzoate functionalized MSNs. Additionally, the successful formation of MSN-Bn **1** was also confirmed by solid-state ^{13}C NMR measurements. As shown in Figure 3 (B), the ^{13}C CP/MAS NMR of MSN-Bn **1** showed a peak at 163.7 ppm corresponding to the carbonyl carbon, and another peak at 128.1 ppm assigned to the phenyl carbon atoms while those at 54.6, 40.4, 18.5 and 6.9 ppm are assigned to the benzylic and the propyl carbon atoms, respectively. The ^{13}C CP/MAS NMR of **1** showed no peaks for the methyl carbon of the benzoate derivative **2**, confirming the complete hydrolysis of the ester **2** to form MSNs-Bn **1**.

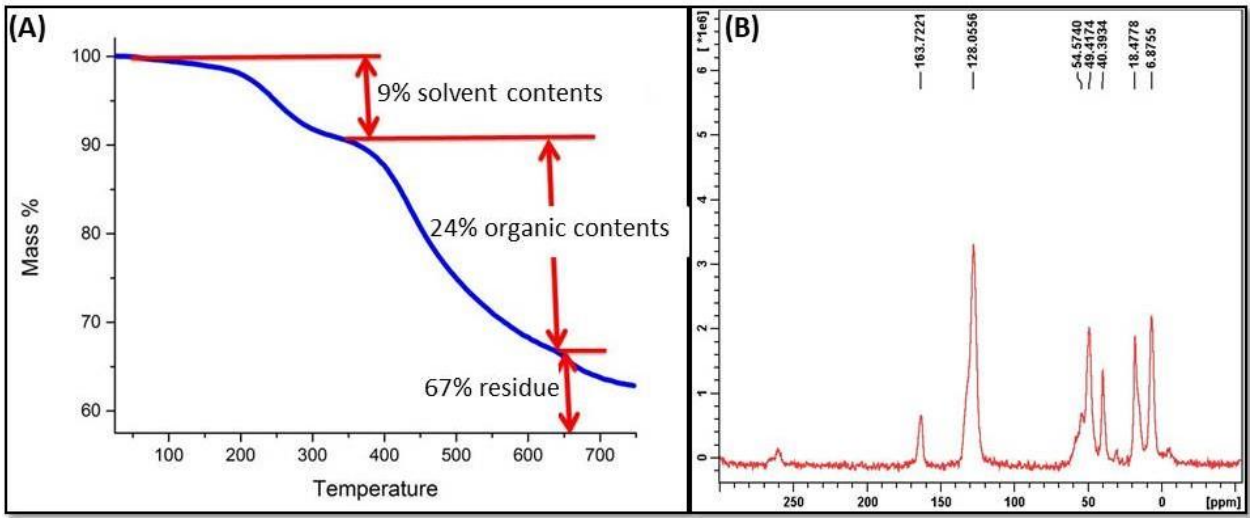

Fig. 3 (A) Thermogravimetric analysis (TGA) curve of **2** displaying the mass percentage of each component of **2**, (B) ^{13}C CP/MAS NMR of MSN-Bn **1**.

With MSNs-Bn **1** in hand, we investigated its tendency to encapsulate and release a payload in response to a pH change (Figure 4). To do this, Hoechst 33342 dye (as a drug model) was added to a suspension of **1** in water and the mixture was stirred overnight to ensure the complete encapsulation of Hoechst dye inside MSNs-Bn nanopores to form **4** (Figure 4A). Subsequently, meso-tetrakis(N-methylpyridinium-4-yl)porphyrin (TMPyP) (as a gatekeeper) was added to the dye-loaded MSNs-Bn in order to close the nanopores orifices of **1**. At pH=7.5, the majority of the benzoic acid moieties of **1** exist as carboxylate anions.

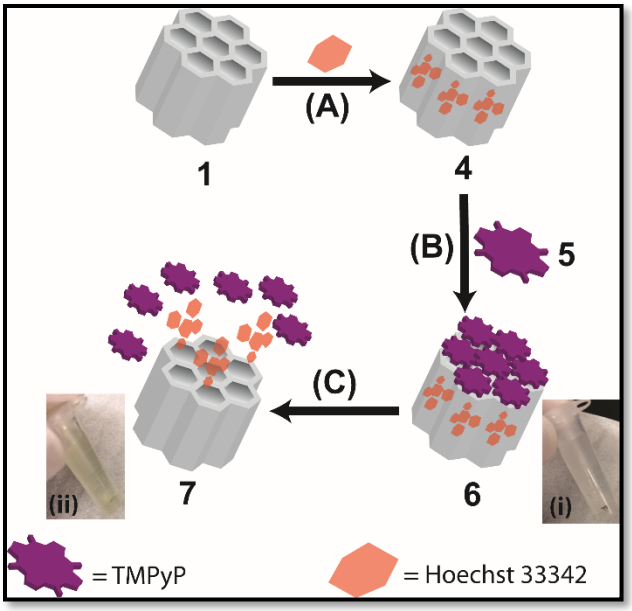

Fig. 4 A graphical representation of (A) Hoechst 33342 dye loading to MSNs-Bn **1** nanopores; (B) Capping of **1** nanopores orifices with TMPyP **5**; and (C) Release of Hoechst 33342 from **1** upon pH change to 4.5. (Images i and ii show the clear and coloured supernatant observed for the (TMPyP) capped Hoechst 33342 loaded MSNs-Bn **1** in buffered solutions at pH 7.5 and 4.5, respectively).

Consequently, and upon the addition of the cationic TMPyP, the electrostatic interactions between the negatively charged nanoparticles surface and the positively charged TMPyP result in the capping of MSNs-Bn nanopores to form **6** (Figure 4B). Once the pH is changed to 4.5, the majority of the benzoic acid on the surface of **1** exists as –COOH with no capability to interact with the capping agent (TMPyP) leading to the release of the gatekeepers followed by the release of Hoechst dye (Figure 4C).

The efficiency of capping MSN-Bn nanopores with TMPyP to form **6**, as well as the pH stimulus release were monitored by steady state fluorescence measurements as shown in Figure 5. The absence of leakage after capping the nanopores of **1** with TMPyP (Figure 4B) was confirmed by the negligible emission recorded after the excitation (at 350 nm) of a portion the supernatant of **6** in water at pH=7.5 at various time intervals. On the other hand, upon changing the pH of the solution to 4.5, excitation of a portion of the supernatant of **6** resulted in a strong emission from the Hoechst payload as shown in Figure 5 due to the release of Hoechst dye as a result of disrupting the electrostatic interactions between the gatekeepers and carboxylate anions at the surface of MSNs-Bn **1**.

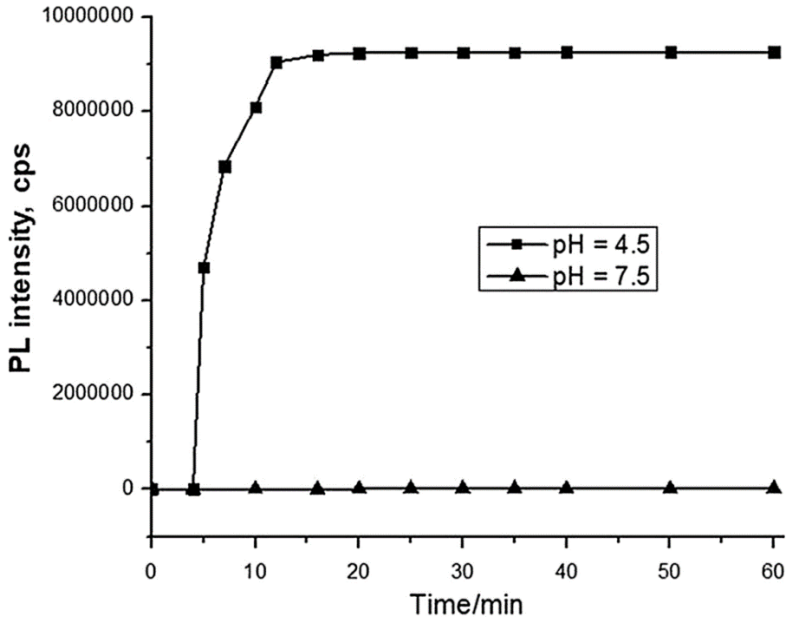

Fig. 5. The release of Hoechst 33342 from the pH-responsive mesoporous silica nanoparticles assembled by TMPyP and MSN-Bn by monitoring the PL intensity of the supernatant at certain interval time in different pH condition (PL excitation wavelength = 350 nm).

The PL measurement confirm the release of Hoechst 33342 at acidic pH 4.5. After complete release, the total weight percent of the entrapped Hoechst 33342 can be quantified through UV−vis absorption measurements of the solution supernatant of Hoechst loaded MSNs-Bn **1**. The delivery capacity of MSNs-Bn **1** was estimated to be 2% weight of Hoechst 33342.

4 Conclusions

In conclusion, we demonstrated the synthesis and characterization of a new mesoporous silica nanoparticle (MSN) derivative, namely, a benzoic acid functionalized MSNs. In addition, the use of MSNs-Bn as a pH responsive drug delivery vehicle – by exploiting ionic self-assembly between the carboxylate groups on the surface of MSNs-Bn and the positively charged meso-tetrakis(N-methylpyridinium-4-yl)porphyrin (TMPyP) – was investigated. MSNs-Bn was first loaded with Hoechst 33342 (as a drug model), at pH=7.5, the formation of carboxylate anions at the surface of MSNs enables electrostatic interactions with the cationic TMPyP resulting in the capping of the silica nanopores. Upon changing the pH to 4.5, these electrostatic interactions were disrupted owing to the protonation of the carboxylate anions thus allowing the release of the encapsulated drug. The reported approach combines in a single particle the photodynamic activity of TMPyP

with the tendency of MSNs-Bn to encapsulate another chemo-therapeutic drug, thus presenting new avenues for synergistic chemo-photodynamic therapy for the treatment of cancer.

Acknowledgements

The authors acknowledge the financial support of King Abdullah University of Science and Technology (KAUST). The generous support of Prof. Osman M. Bakr is highly appreciated by the authors.

Compliance with ethical standards

Conflict of interest. All authors declare that they have no conflict of interest.

References

1. D. E. J. G. J. Dolmans, D. Fukumura, and R. K. Jain, Nat. Rev. Cancer **3**, 380 (2003).
2. A. P. Castano, P. Mroz, and M. R. Hamblin, Nat. Rev. Cancer **6**, 535 (2006).
3. J. P. Celli, B. Q. Spring, I. Rizvi, C. L. Evans, K. S. Samkoe, S. Verma, B. W. Pogue, and T. Hasan, Chem. Rev. **110**, 2795 (2010).
4. A. F. dos Santos, D. R. Q. de Almeida, L. F. Terra, M. S. Baptista, and L. Labriola, J. Cancer Metastasis Treat. **5**, 25 (2019).
5. X. Shi, C. Y. Zhang, J. Gao, and Z. Wang, WIREs Nanomedicine Nanobiotechnology **11**, e1560 (2019).
6. R. T. Wheelhouse, D. Sun, H. Han, F. X. Han, and L. H. Hurley, J. Am. Chem. Soc. **120**, 3261 (1998).
7. F. X. Han, R. T. Wheelhouse, and L. H. Hurley, J. Am. Chem. Soc. **121**, 3561 (1999).
8. G. N. Parkinson, R. Ghosh, and S. Neidle, Biochemistry **46**, 2390 (2007).
9. S. Tada-Oikawa, S. Oikawa, J. Hirayama, K. Hirakawa, and S. Kawanishi, Photochem. Photobiol. **85**, 1391 (2009).
10. M. Ethirajan, Y. Chen, P. Joshi, and R. K. Pandey, Chem. Soc. Rev. **40**, 340 (2010).
11. C. Wei, G. Jia, J. Yuan, Z. Feng, and C. Li, Biochemistry **45**, 6681 (2006).
12. E. Ruggiero and S. N. Richter, Nucleic Acids Res. **46**, 3270 (2018).

13. M. I. Umar, D. Ji, C.-Y. Chan, and C. K. Kwok, Molecules **24**, 2416 (2019).
14. C. Pérez-Arnaiz, N. Busto, J. Santolaya, J. M. Leal, G. Barone, and B. García, Biochim. Biophys. Acta BBA - Gen. Subj. **1862**, 522 (2018).
15. Y. Ma, K. Iida, and K. Nagasawa, Biochem. Biophys. Res. In Press. Commun. (2020).
16. A. Ferino, G. Nicoletto, F. D'Este, S. Zorzet, S. Lago, S. N. Richter, A. Tikhomirov, A. Shchekotikhin, and L. E. Xodo, J. Med. Chem. **63**, 1245 (2020).
17. K. K. Cotí, M. E. Belowich, M. Liong, M. W. Ambrogio, Y. A. Lau, H. A. Khatib, J. I. Zink, N. M. Khashab, and J. Fraser Stoddart, Nanoscale **1**, 16 (2009).
18. Q. He and J. Shi, J. Mater. Chem. **21**, 5845 (2011).
19. C. Coll, A. Bernardos, R. Martínez-Máñez, and F. Sancenón, Acc. Chem. Res. **46**, 339 (2013).
20. M. Manzano and M. Vallet-Regí, Adv. Funct. Mater. **30**, 1902634 (2020).
21. J. Wen, K. Yang, F. Liu, H. Li, Y. Xu, and S. Sun, Chem. Soc. Rev. **46**, 6024 (2017).
22. J. L. Vivero-Escoto, I. I. Slowing, B. G. Trewyn, and V. S.-Y. Lin, Small **6**, 1952 (2010).
23. W. Chen, C. A. Glackin, M. A. Horwitz, and J. I. Zink, Acc. Chem. Res. **52**, 1531 (2019).
24. R. R. Castillo, D. Lozano, B. González, M. Manzano, I. Izquierdo-Barba, and M. Vallet-Regí, Expert Opin. Drug Deliv. **16**, 415 (2019).
25. C.-A. Cheng, T. Deng, F.-C. Lin, Y. Cai, and J. I. Zink, Theranostics **9**, 3341 (2019).
26. N. Iturrioz-Rodríguez, M. A. Correa-Duarte, and M. L. Fanarraga, Int. J. Nanomedicine **14**, (2019).
27. A. Watermann and J. Brieger, Nanomaterials **7**, 189 (2017).
28. Z. Li, Y. Zhang, and N. Feng, Expert Opin. Drug Deliv. **16**, 219 (2019).
29. M. Frasconi, Z. Liu, J. Lei, Y. Wu, E. Strekalova, D. Malin, M. W. Ambrogio, X. Chen, Y. Y. Botros, V. L. Cryns, J.-P. Sauvage, and J. F. Stoddart, J. Am. Chem. Soc. **135**, 11603 (2013).
30. S. A. Mackowiak, A. Schmidt, V. Weiss, C. Argyo, C. von Schirnding, T. Bein, and C. Bräuchle, Nano Lett. **13**, 2576 (2013).
31. H. Li, L.-L. Tan, P. Jia, Q.-L. Li, Y.-L. Sun, J. Zhang, Y.-Q. Ning, J. Yu, and Y.-W. Yang, Chem. Sci. **5**, 2804 (2014).
32. M. S. Moorthy, S. Bharathiraja, P. Manivasagan, Y. Oh, B. Jang, T. T. V. Phan, and J. Oh, J. Porous Mater. **25**, 119 (2018).
33. Y. Zhou, L.-L. Tan, Q.-L. Li, X.-L. Qiu, A.-D. Qi, Y. Tao, and Y.-W. Yang, Chem. – Eur. J. **20**, 2998 (2014).

34. D. Tarn, D. P. Ferris, J. C. Barnes, M. W. Ambrogio, J. F. Stoddart, and J. I. Zink, Nanoscale **6**, 3335 (2014).
35. M. Deniz Yilmaz, M. Xue, M. W. Ambrogio, O. Buyukcakir, Y. Wu, M. Frasconi, X. Chen, M. S. Nassar, J. Fraser Stoddart, and J. I. Zink, Nanoscale **7**, 1067 (2015).
36. M. Aquib, M. A. Farooq, P. Banerjee, F. Akhtar, M. S. Filli, K. O. Boakye-Yiadom, S. Kesse, F. Raza, M. B. J. Maviah, R. Mavlyanova, and B. Wang, J. Biomed. Mater. Res. A **107**, 2643 (2019).
37. M. S. Moorthy, G. Hoang, P. Manivasagan, S. Mondal, T. T. Vy Phan, H. Kim, and J. Oh, J. Porous Mater. **26**, 217 (2019).
38. M. Hamzehloo, J. Karimi, K. Aghapoor, H. Sayahi, and H. R. Darabi, J. Porous Mater. **25**, 1275 (2018).
39. X. Jia, Z. Yang, Y. Wang, Y. Chen, H. Yuan, H. Chen, X. Xu, X. Gao, Z. Liang, Y. Sun, J.-R. Li, H. Zheng, and R. Cao, ChemMedChem **13**, 400 (2018).
40. W. Lei, C. Sun, T. Jiang, Y. Gao, Y. Yang, Q. Zhao, and S. Wang, Mater. Sci. Eng. C **105**, 110103 (2019).
41. X. Li, C. Xie, H. Xia, and Z. Wang, Langmuir **34**, 9974 (2018).
42. Z. Song, Y. Liu, J. Shi, T. Ma, Z. Zhang, H. Ma, and S. Cao, Mater. Sci. Eng. C **83**, 90 (2018).
43. L. Jin, Q.-J. Huang, H.-Y. Zeng, J.-Z. Du, S. Xu, and C.-R. Chen, Microporous Mesoporous Mater. **274**, 304 (2019).
44. S. S. Park, M. H. Jung, Y.-S. Lee, J.-H. Bae, S.-H. Kim, and C.-S. Ha, Mater. Des. **184**, 108187 (2019).
45. K. Cheng, Y. Zhang, Y. Li, Z. Gao, F. Chen, K. Sun, P. An, C. Sun, Y. Jiang, and B. Sun, J. Mater. Chem. B **7**, 3291 (2019).
46. F. Zhao, C. Zhang, C. Zhao, W. Gao, X. Fan, and G. Wu, Colloids Surf. B Biointerfaces **179**, 352 (2019).
47. B. Tian, S. Liu, S. Wu, W. Lu, D. Wang, L. Jin, B. Hu, K. Li, Z. Wang, and Z. Quan, Colloids Surf. B Biointerfaces **154**, 287 (2017).
48. C. T. H. Nguyen, R. I. Webb, L. K. Lambert, E. Strounina, E. C. Lee, M.-O. Parat, M. A. McGuckin, A. Popat, P. J. Cabot, and B. P. Ross, ACS Appl. Mater. Interfaces **9**, 9470 (2017).
49. C. Yang, Z. Shi, C. Feng, R. Li, S. Luo, X. Li, and L. Ruan, Macromol. Biosci. **20**, 2000034 (2020).

50. M. Gisbert-Garzarán, M. Manzano, and M. Vallet-Regí, Bioengineering **4**, 3 (2017).
51. H. Wang, F. Li, C. Du, H. Wang, R. I. Mahato, and Y. Huang, Mol. Pharm. **11**, 2600 (2014).
52. H. Wang, Q. Guo, Y. Jiang, E. Liu, Y. Zhao, H. Wang, Y. Li, and Y. Huang, Adv. Funct. Mater. **23**, 6068 (2013).
53. X. Deng, Y. Liang, X. Peng, T. Su, S. Luo, J. Cao, Z. Gu, and B. He, Chem. Commun. **51**, 4271 (2015).
54. S. Zhang, H. Lv, J. Zhao, M. Cheng, and S. Sun, Nanotechnology **30**, 265102 (2019).
55. J. Wang, Y. Zhong, X. Wang, W. Yang, F. Bai, B. Zhang, L. Alarid, K. Bian, and H. Fan, Nano Lett. **17**, 6916 (2017).
56. E. Secret, M. Maynadier, A. Gallud, A. Chaix, E. Bouffard, M. Gary-Bobo, N. Marcotte, O. Mongin, K. E. Cheikh, V. Hugues, M. Auffan, C. Frochot, A. Morère, P. Maillard, M. Blanchard-Desce, M. J. Sailor, M. Garcia, J.-O. Durand, and F. Cunin, Adv. Mater. **26**, 7643 (2014).
57. T.-W. Kim, P.-W. Chung, and V. S.-Y. Lin, Chem. Mater. **22**, 5093 (2010).
58. R. C. Fuson and H. G. Cooke, J. Am. Chem. Soc. **62**, 1180 (1940).